

Thermoradiative Power Conversion from HgCdTe Photodiodes and Their Current–Voltage Characteristics

Michael P. Nielsen,[‡] Andreas Pusch,[‡] Muhammad H. Sazzad, Phoebe M. Pearce, Peter J. Reece, and Nicholas J. Ekins-Daukes*



Cite This: *ACS Photonics* 2022, 9, 1535–1540



Read Online

ACCESS |

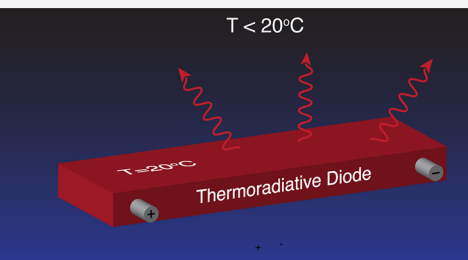
Metrics & More

Article Recommendations

Supporting Information

ABSTRACT: The thermoradiative diode represents the less well-known symmetric counterpart to solar photovoltaics that instead utilizes the net emission of light rather than absorption to generate power. While there are promising theoretical predictions for its application in night-sky power generation and waste heat recovery, the current technological limits have not been explored. Here we explicitly measure the electro-optical characteristics of HgCdTe photodiodes across a range of bandgap energies in both thermoradiative and photovoltaic operation, supported by theoretical calculations that include critical nonradiative processes. At a temperature differential of only 12.5 °C, we measure a peak thermoradiative electrical power density of 2.26 mW/m² for a photodiode emitting near 4.7 μm, with an estimated radiative efficiency of 1.8%. Our results highlight the need for achieving high radiative efficiencies with mid-infrared semiconductors to deliver on the promise of thermoradiative power generation.

KEYWORDS: *thermoradiative power, thermophotovoltaics, MIR photodiodes, HgCdTe photodiodes*



Radiative heat transfer is commonly described as a process driven only by differences in temperature between an absorber and an emitter.¹ However, in semiconductor devices radiative heat transfer gains an additional degree of freedom via an electrical bias. The process of electroluminescence describes radiative emission from a forward biased semiconductor diode that greatly exceeds the emission at equilibrium.^{2,3} The reverse process is less well-known, in which a reverse-biased mid-infrared (MIR) semiconductor diode emits less radiation than at equilibrium in a process known as “negative luminescence”.^{4,5} Thermodynamically, the phenomena of forward-biased electroluminescence (EL) and reverse-biased negative luminescence (NL) form the operating basis for an optoelectronic heat-pump⁶ and optoelectronic refrigeration.⁷ In the case of a photovoltaic device, radiative transfer from a high-temperature heat source (e.g., sunlight) to the semiconductor diode at a lower temperature results in the formation of a voltage. Remarkably, the symmetric counterpart to the photovoltaic device has only recently been identified: the thermoradiative harvester^{8,9,23} that generates electrical power by radiating light from a warm ambient into cold surroundings. This counterintuitive device derives power by rejecting more entropy via radiative emission than is supplied by the incoming heat flow from the surrounding thermal reservoir.^{10,11,24} One of the applications for this thermoradiative diode is night-sky power generation,¹³ extracting a small amount of electrical power from the radiative loss from the planet into the cold universe. To date this has only been demonstrated via direct radiative cooling^{14–16} and then

exploiting the resultant thermal gradient to generate power.¹⁷ Other applications of the thermoradiative diode include waste heat recovery (both terrestrial and in space)^{12,18,19} and in combination with photovoltaics.^{20–22}

In this work we demonstrate direct thermoradiative power conversion using MIR semiconductor diodes exposed to a cold environment with the results supported by optoelectronic modeling. We thus establish the device as the emissive counterpart to a p–n junction photovoltaic device. In Figure 1 we illustrate the current and voltage (*I*–*V*) characteristics of a typical photovoltaic and thermoradiative diode. A photovoltaic cell conventionally operates with a negative short-circuit current (I_{sc}) and positive open-circuit voltage (V_{oc}), while the thermoradiative device operates with a positive short circuit current and negative open-circuit voltage. Strandberg²³ calculated the *I*–*V* curve of an ideal diode exposed to a cold surface in the radiative limit, from which it can be determined that the electrical power from a radiative exchange between 300 and 3 K could reach up to 54.8 W/m².¹¹ In the radiative limit, the maximum power is always obtained at a reverse bias voltage close to the thermal voltage.²⁴ However, in practice, nonradiative processes in MIR diodes will reduce the absolute

Received: February 8, 2022

Published: May 9, 2022



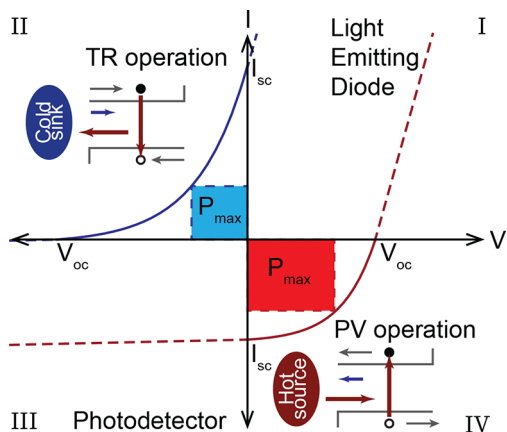


Figure 1. The four current–voltage operating quadrants for a photodiode: (I) Light-emitting diode (LED); (II) Thermoradiative (TR); (III) Photodetector (PD); and (IV) Photovoltaic (PV) operation, with a representative depiction (not to scale) of the interplay in emission between an arbitrary photodiode and either a hot source or a cold sink.

value of the open circuit voltage to values far below the thermal voltage, resulting in a linear I – V curve that is defined by a dynamic resistance in the power generating quadrant.^{24,25} Santhanam et al.²⁶ estimated the achievable power from a MIR diode by exposing it to a cold surface and measuring only the short circuit current. The dark dynamic resistance was then used to estimate the open circuit voltage, but the full thermoradiative I – V behavior was not reported. Here we explicitly measure the power generating I – V curves by varying the resistance of a variable load connected in series to MIR diodes exposed to both cold and warm surfaces. We also show that reverse-bias “negative” luminescence is a requirement for thermoradiative generation that represents the spectroscopic signature of a viable thermoradiative device. Our experimental

results are supported by theoretical calculations that account for the effect of the diode immersion lens and nonradiative processes, and additionally indicate how the optimum thermoradiative diode emission energy is dependent on both the balance of nonradiative processes and the temperature differential.

The full four quadrant current–voltage characteristics of a photodiode in different radiative configurations are shown in Figure 1. In each case, the current–voltage characteristics for a diode of active area A_D can be calculated via:²⁴

$$J(V, T_D, T_S) = \frac{q}{A_D} \phi_{\text{tot}}(T_D, V) - \frac{q}{A_D} \phi_{\text{tot}}(T_S, 0) + J_{\text{Aug}}(T_D, V) + J_{\text{SRH}}(T_D, V) \quad (1)$$

where ϕ_{tot} represents an incoming or outgoing photon flux, the temperature of the device T_D , which may be larger or smaller than the temperature of the source/sink T_S , and the voltage of the device may be negative or positive. Parasitic Auger (J_{Aug}) and Shockley-Read Hall (J_{SRH}) currents depend on thickness, bandgap, doping density, and material quality of the device, while the radiative flux from and into a planar device can be approximated by the generalized Planck equation²⁷ using optoelectronic reciprocity²⁸ as the following:

$$\phi_{\text{tot}}^{\text{planar}}(T_D, V) = \frac{4\pi}{c^2} \int_0^\infty \int_0^{\pi/2} \frac{\omega^2 EQE(\omega, \beta)}{e^{\hbar\omega - qV/k_B T_D}} d\beta d\omega \quad (2)$$

where k_B is the Boltzmann constant. The frequency (ω) and angle (β) dependent external quantum efficiency (EQE) is the key quantity that determines the radiative exchange of the diode with its environment. The familiar photovoltaic device, operating in quadrant IV, relies upon net absorption of photons from a hot source, whereas the thermoradiative device operating in quadrant II draws current into the diode upon net emission of radiation into a cold sink. For the photovoltaic device, the absorption of light gives rise to an excess

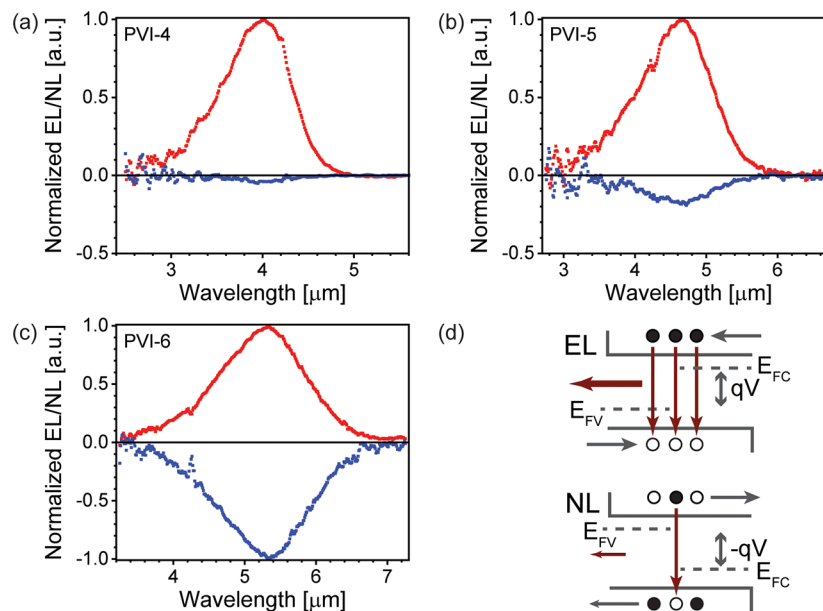


Figure 2. Electroluminescence and negative luminescence of mid-infrared photodiodes. Spectrally resolved electroluminescence and negative luminescence signals normalized to the peak electroluminescence from (a) PVI-4 (nominally 4 μm photodiode), (b) PVI-5 (nominally 5 μm photodiode), and (c) PVI-6 (nominally 6 μm photodiode) at equivalent reverse and forward bias. (d) The respective carrier densities and quasi-Fermi levels responsible for the radiative processes are depicted schematically for electroluminescence and negative luminescence.

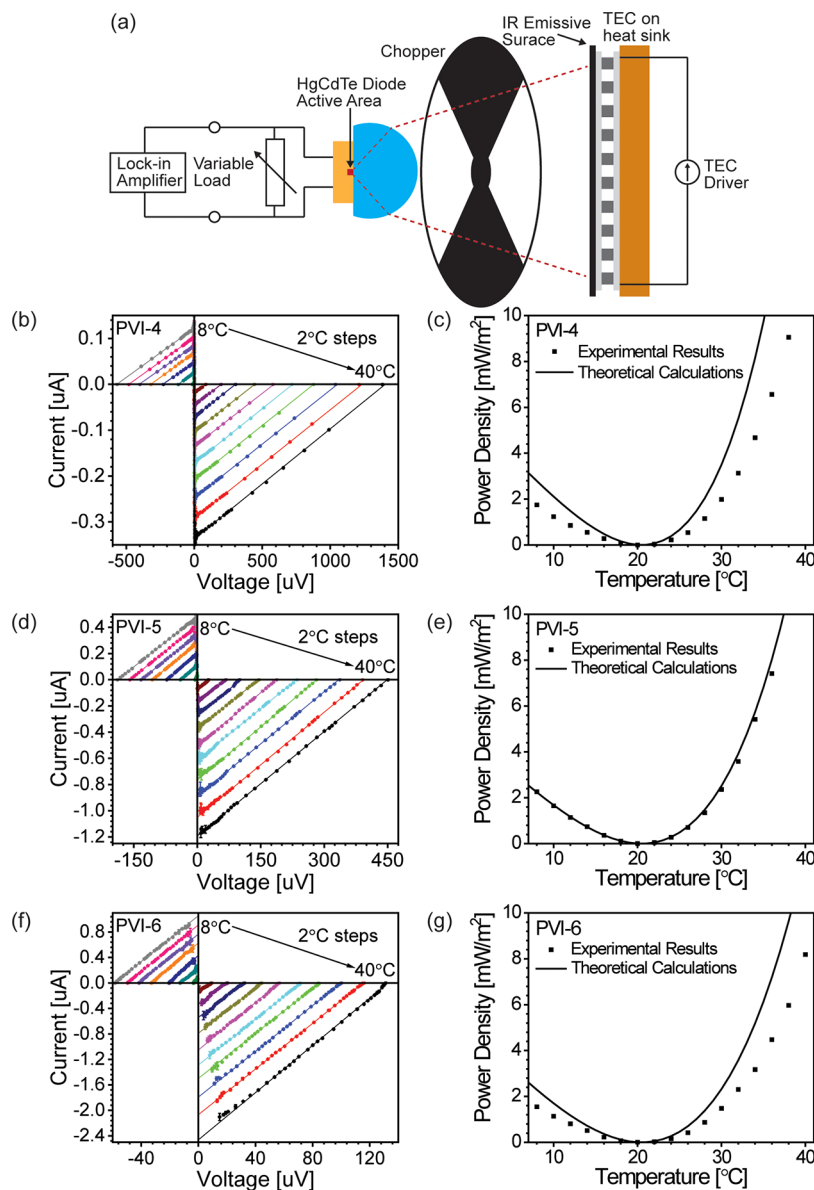


Figure 3. Variable load current–voltage power generation measurements. (a) Schematic representation of the variable load current–voltage power generation measurements. Variable loaded current–voltage measurements in photovoltaic and thermoradiative operation at 20.5 °C for the (b) PVI-4, (d) PVI-5, and (f) PVI-6 photodiodes with linear fits to the data. Extracted power density as a function of emissive surface temperature compared to theoretical calculations for the $0.1 \times 0.1 \text{ mm}^2$ (c) PVI-4, (e) PVI-5, and (g) PVI-6 photodiodes.

concentration of electron (n) and hole (p) charge carriers, resulting in a positive splitting of the quasi-Fermi energies and hence positive voltage. This leads to enhanced radiative recombination that will proceed in proportion to the product np . In the radiative limit, the quasi-Fermi energy splitting equals the (positive) V_{oc} when radiative recombination matches the photogeneration rate. In a thermoradiative diode, a net radiative current is lost from the device at I_{sc} . Connecting a finite load to the thermoradiative device will result in the diode becoming reverse biased, with the carrier concentrations lower than at equilibrium. The negative open circuit voltage is the point where, in the radiative limit, the emitted flux matches the absorbed flux from the cold surroundings. This reduction in radiative recombination, previously observed from MIR LEDs,^{4,5,7} is known as “negative luminescence” (NL) and is wholly consistent with eq 2 when V is negative. The presence of NL in a thermoradiative diode at

reverse bias provides spectroscopic confirmation that thermoradiative power generation can take place and reveals the photon emission wavelength range responsible.

We report results from three mid-infrared HgCdTe (MCT) photodiodes from VIGO System: PVI-4-1x1-TO39-wNone-36, PVI-5-1x1-TO39-wNone-36, and PVI-6-1x1-TO39-wNone-36. Each photodiode has a $0.1 \times 0.1 \text{ mm}^2$ physical area with a monolithically integrated GaAs hyperhemispherical lens for in/out coupling of radiation and nominal band-edges of 4, 5, and 6 μm , respectively; additional details are presented in the *Supporting Information*, including their physical and optoelectronic properties. In the radiative limit, without non-radiative processes, diodes with lower bandgap energies lead to increased power generation. Theoretically, the PVI-6 should be the most promising of the diodes since the NL range is closest to the peak photon flux of the blackbody emission at room temperature (12.5 μm), with the other two higher bandgap

diodes expected to deliver lower power output. Figure 2 illustrates that all three diodes clearly show both electroluminescence and negative luminescence according to the applied bias conditions at room temperature (20.5 °C or 293.65 K), with the relative strength of EL/NL scaling with bandgap. Importantly, the EL and NL spectra from the diodes closely resemble one another, with only a small spectral shift attributed to the Moss–Burstein effect in forward bias.⁴ Further details and additional EL/NL measurements can be found in the [Supporting Information](#), along with the calculated emission spectra of the photodiodes.

To demonstrate power generation, the photodiodes were aligned facing a mid-infrared-emissive thermally controlled surface. Due to the small currents and voltages generated from these diodes, the photodiodes were directly connected to a variable load, and the resultant voltage was measured via lock-in detection using a chopper. By ensuring the photodiode only sees the emissive surface or the chopper blade (also coated in the same emissive surface albeit at ambient temperature), the photocurrent could be directly measured by the voltage across the load combined with the load resistance. The phase of the measured signal indicated the direction of the photocurrent and thus the operating mode of the photodiode. Finally, by varying the load between 7 Ω and 10 kΩ, the current–voltage characteristics could be measured, enabling direct determination of the maximum power point at every temperature differential between the photodiode and the emissive surface. Both the chopper blade and the photodiode were operated at ambient temperature (20.5 ± 0.1 °C). The experimental schematic is shown in Figure 3a, with further details presented in the [Supporting Information](#).

Figure 3bdf shows the variable loaded current–voltage measurements in photovoltaic and thermoradiative modes for the photodiodes at a variety of temperatures of the emissive surface. As expected for a diode operating at voltages much smaller than the thermal voltage ($V_{\text{thermal}} = kT/q = 25.3$ mV exceeds the measured voltage range by an order of magnitude), this results in a series of linear I – V curves with characteristic dynamic resistances (R_D) of 4.4 kΩ (PVI-4), 380 Ω (PVI-5), and 55 Ω (PVI-6) extracted from a linear fit to the data, in agreement with dark I – V measurements (see [Supporting Information](#)) at small voltages far from rectification. The experimentally extracted power densities (Figure 3c,e,g) closely match our theoretical calculations, especially for PVI-5, and were calculated via (valid for linear I – V curves only) the following:

$$P_{\text{density}} = \frac{1}{4} I_{\text{sc}} V_{\text{oc}} / A_D \quad (3)$$

Our theoretical model accounts for the known external quantum efficiencies and dynamic resistance of the photodiodes (which reflect the radiative as well as the nonradiative processes of Auger recombination/generation and Shockley–Read–Hall (SRH) recombination/generation), the implications of the monolithically integrated hyperhemispherical GaAs lens on top of the 0.1 × 0.1 mm² active diode area, and the balance of the photon flux from the diode to the environment and vice versa given the known temperature differential. Note that the use of the hyperhemispherical lenses would prevent close packing of these diodes for large area applications. Full details of these theoretical calculations are provided in the [Supporting Information](#).

These results show a strong dependence of the potential power generation on the temperature differential between the photodiode and the emissive surface. Examining how the generated power scales with bandgap makes it clear that there is a balance between external radiative efficiency (which increases with an increasing bandgap energy) and the overlap of the temperature-dependent blackbody spectra with the photodiode's absorption. It is possible to estimate the external radiative efficiencies of the photodiodes by comparing the known dynamic resistance (a measure of radiative and nonradiative processes in the device) with the calculated radiative flux as:

$$\eta_{\text{rad}} = R_D q^2 A_D \phi_{\text{tot}}(T_D, 0) / [k_B T_D] \quad (4)$$

where $\phi_{\text{tot}}(T_D, 0)$ is the total externally emitted photon flux from the diode at short circuit. ϕ_{tot} is determined using ray tracing to include the effect of the hyperhemispherical lens that both enhances the total emission compared to a flat surface (as described by [eq 2](#)) approximately by the square of the refractive index (n_{lens}^2) and additionally focuses it to a narrower emission cone²⁹ (for more details, see the [Supporting Information](#)). It should be noted that for a far-field application (such as night-sky power generation), the index matched hyperhemispherical lens represents the ideal case, but for near-field applications (including waste-heat recovery) alternate approaches could be realized to enhance the thermal photon transfer^{12,30} (known as near-field radiative heat transfer) as has been explored with thermophotovoltaic devices³¹ and radiative cooling.³² Further details on this calculation can be found in the [Supporting Information](#). We estimate the external radiative efficiency to be 0.8%, 1.8%, and 6.5% for the PVI-6, PVI-5, and PVI-4 photodiodes, respectively, with the achievable power from these devices scaling linearly with radiative efficiency in the regime of low radiative efficiency.²⁴ As can be seen in Figure 3, the theoretical power predictions demonstrate that the PVI-4 photodiode should outperform both the PVI-5 and PVI-6 photodiodes in this temperature range due to its significantly lower nonradiative recombination. However, it was the PVI-5 photodiode's short circuit current that most closely matched the theoretical predictions and, thus, outperformed the other photodiodes.

Using our theoretical model for the emitted photon flux, we estimate the extractable electrical power density for our MCT thermoradiative diodes over a range of emissive environment temperatures, as shown in Figure 4. Given the trade-off when balancing nonradiative recombination and the overlap of the blackbody spectra with the photodiode's absorption, at different radiative environment temperatures a different photodiode produces the most power. In this case, above 258 K (~−15 °C) the PVI-4 photodiode is expected to deliver the most power, whereas below 258 K the PVI-6 is expected to deliver the most power. Extending the model to an exchange between 293 K (~20 °C) and space (for night sky power generation) at 3 K results in an achievable power density of 15.1, 15.0, and 19.4 mW/m² for the PVI-4, PVI-5, and PVI-6 photodiodes, respectively, when ignoring atmospheric absorption. The saturation in the power generation curves in Figure 4 is more pronounced for higher bandgaps because the blackbody spectral power density at shorter wavelengths decreases more quickly with decreasing temperature than at longer wavelengths. This saturation of the potential power generation indicates that extreme temperature differentials are

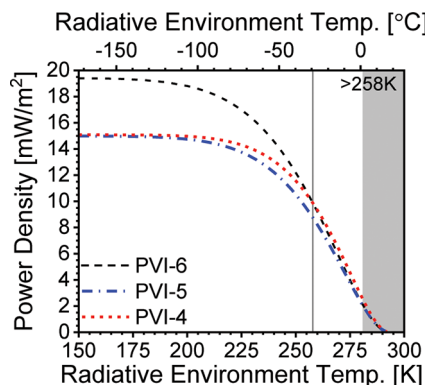


Figure 4. Extending thermoradiative power generation to larger temperature differentials. Theoretical extractable power densities in thermoradiative operation between photodiodes at 293 K (~20 °C) and a radiative environment at a range of temperatures. The shaded region represents the temperature range covered by the experimental measurements.

not necessary for thermoradiative operation. Additionally, these results show that the neglect of nonradiative recombination in the radiative limit not only overestimates the achievable power, but also strongly misleads any optimal device design. We emphasize that for any practical device, the choice of bandgap and device architecture must account for these inevitable nonradiative processes. For comparison, in the radiative limit the extractable power densities would strongly vary with bandgap for the 293 to 3 K temperature exchange, starting at 3.5 W/m² for the PVI-6 diode and decreasing to 1.2 and 0.34 W/m² for the PVI-5 and PVI-4 diodes, respectively.

Here we have measured the current–voltage characteristics of HgCdTe mid-infrared photodiodes operating in thermoradiative mode directly, and thus explicitly determine the electrical power without assumptions. We further demonstrate the same diodes operating in thermophotovoltaic mode, and show how negative luminescence provides the spectroscopic signature of thermoradiative operation. With a temperature differential of only 12.5 °C and the PVI-5 photodiode temperature at 20.5 °C, we have demonstrated a thermoradiative electrical power density of 2.26 mW/m², supported by quantitative theoretical calculations that account for the physical and optoelectronic properties of this photodiode. By linking the experimental results to modeling, we provide a realistic method for predicting thermoradiative power generation and indicate the importance of radiative efficiency. Furthermore, we demonstrate that careful consideration of the balance between nonradiative recombination and the overlap of the blackbody spectra with the photodiode’s absorption is key to determining what bandgap of photodiode will generate the most power at a given temperature exchange, with larger temperature differences favoring photodiodes with lower bandgap energies. Our theoretical model established that the external radiative efficiencies from our diodes range from 0.8% for the lower band gap to 6.5% for the higher band gap. In order to realize the promise of thermoradiative power conversion on the order of W/m², extremely high radiative efficiencies from mid-IR semiconductors will be required.

ASSOCIATED CONTENT

Supporting Information

The Supporting Information is available free of charge at <https://pubs.acs.org/doi/10.1021/acsphtronics.2c00223>.

Additional details on the MIR photodiodes, experimental details, and modeling of the optical/electrical properties of the MIR photodiodes; Figures S1–S9; Equations S1–S17; Supplementary references 1–6 (PDF)

AUTHOR INFORMATION

Corresponding Author

Nicholas J. Ekins-Daukes – School of Photovoltaic and Renewable Energy Engineering, University of New South Wales, Sydney, NSW 2052, Australia; [0003-1875-9739](https://orcid.org/0000-0003-1875-9739); Email: nekins@unsw.edu.au

Authors

Michael P. Nielsen – School of Photovoltaic and Renewable Energy Engineering, University of New South Wales, Sydney, NSW 2052, Australia; [0000-0002-0457-7208](https://orcid.org/0000-0002-0457-7208)

Andreas Pusch – School of Photovoltaic and Renewable Energy Engineering, University of New South Wales, Sydney, NSW 2052, Australia

Muhammad H. Sazzad – School of Photovoltaic and Renewable Energy Engineering, University of New South Wales, Sydney, NSW 2052, Australia; [0000-0002-4699-6937](https://orcid.org/0000-0002-4699-6937)

Phoebe M. Pearce – ARC Centre of Excellence in Exciton Science, School of Photovoltaic and Renewable Energy Engineering, University of New South Wales, Sydney, NSW 2052, Australia; Department of Physics, University of Cambridge, Cambridge CB3 0HE, United Kingdom

Peter J. Reece – School of Physics, University of New South Wales, Sydney, NSW 2052, Australia; [0000-0003-4852-3735](https://orcid.org/0000-0003-4852-3735)

Complete contact information is available at: <https://pubs.acs.org/10.1021/acsphtronics.2c00223>

Author Contributions

[‡]M.P.N. and A.P. contributed equally to this work. N.J.E.-D. conceived the project. M.P.N. and M.H.S. designed and conducted the experiments and analyzed the results. A.P. developed and produced the analytical device modeling, with ray tracing provided by P.P. P.R. and N.J.E.-D. supervised the project. M.P.N., A.P., and N.J.E.-D. cowrote the manuscript. All authors commented on the manuscript.

Funding

N.J.E.-D. and A.P. are supported by the UNSW SHARP program, M.P.N. is supported by a UNSW Scientia Fellowship, M.H.S. is supported by a UNSW Scientia Studentship, and P.M.P. is supported by a Research Fellowship from the ARC Centre of Excellence for Exciton Science CE170100026.

Notes

The authors declare no competing financial interest.

REFERENCES

- (1) Holman, J. P. *Heat Transfer*, 10th ed.; McGraw-Hill Series in Mechanical Engineering, 2010.
- (2) van Roosbroeck, W.; Shockley, W. Photon-Radiative Recombination of Electrons and Holes in Germanium. *Phys. Rev.* **1954**, *94* (6), 1558.
- (3) Feuerbacher, B.; Wurfel, P. Verification of a Generalised Planck Law by Investigation of the Emission from GaAs Luminescent Diodes. *J. Phys.: Condens. Matter* **1990**, *2* (16), 3803.
- (4) Elliott, C. T. Negative Luminescence and Its Applications. *Philos. Trans. R. Soc. A Math. Phys. Eng. Sci.* **2001**, *359* (1780), 567–579.

- (5) Ashley, T.; Elliott, C. T.; Gordon, N. T.; Phillips, T. J.; Hall, R. S. Applications of Negative Luminescence. *Infrared Phys. Technol.* **1997**, *38* (3), 145–151.
- (6) Sadi, T.; Radevici, I.; Oksanen, J. Thermophotonic Cooling with Light-Emitting Diodes. *Nat. Photonics* **2020**, *14* (4), 205–214.
- (7) Berdahl, P. Radiant Refrigeration by Semiconductor Diodes. *J. Appl. Phys.* **1985**, *58* (3), 1369–1374.
- (8) Byrnes, S. J.; Blanchard, R.; Capasso, F. Harvesting Renewable Energy from Earth's Mid-Infrared Emissions. *Proc. Natl. Acad. Sci. U. S. A.* **2014**, *111* (11), 3927–3932.
- (9) Strandberg, R. Heat to Electricity Conversion by Cold Carrier Emissive Energy Harvesters. *J. Appl. Phys.* **2015**, *118* (21), 215102.
- (10) Boriskina, S. V.; Tong, J. K.; Hsu, W. C.; Liao, B.; Huang, Y.; Chiloyan, V.; Chen, G. Heat Meets Light on the Nanoscale. *Nanophotonics* **2016**, *5* (1), 134–160.
- (11) Buddhiraju, S.; Santhanam, P.; Fan, S. Thermodynamic Limits of Energy Harvesting from Outgoing Thermal Radiation. *Proc. Natl. Acad. Sci. U. S. A.* **2018**, *115* (16), E3609–E3615.
- (12) Tervo, E.; Bagherisereshki, E.; Zhang, Z. Near-Field Radiative Thermoelectric Energy Converters: A Review. *Front. Energy* **2018**, *12* (1), 5–21.
- (13) Deppe, T.; Munday, J. N. Nighttime Photovoltaic Cells: Electrical Power Generation by Optically Coupling with Deep Space. *ACS Photonics* **2020**, *7* (1), 1–9.
- (14) Yin, X.; Yang, R.; Tan, G.; Fan, S. Terrestrial Radiative Cooling: Using the Cold Universe as a Renewable and Sustainable Energy Source. *Science* **2020**, *370* (6518), 786–791.
- (15) Sun, X.; Sun, Y.; Zhou, Z.; Alam, M. A.; Bermel, P. Radiative Sky Cooling: Fundamental Physics, Materials, Structures, and Applications. *Nanophotonics* **2017**, *6* (5), 997–1015.
- (16) Hossain, M. M.; Gu, M. Radiative Cooling: Principles, Progress, and Potentials. *Adv. Sci.* **2016**, *3* (7), 1500360.
- (17) Raman, A. P.; Li, W.; Fan, S. Generating Light from Darkness. *Joule* **2019**, *3* (11), 2679–2686.
- (18) Wang, J.; Chen, C. H.; Bonner, R.; Anderson, W. G. Thermo-Radiative Cell – A New Waste Heat Recovery Technology for Space Power Applications. *AIAA Propuls. Energy Forum Expo* **2019**, 2019, 3977.
- (19) Hsu, W.-C.; Tong, J. K.; Liao, B.; Huang, Y.; Boriskina, S. V.; Chen, G. Entropic and Near-Field Improvements of Thermoradiative Cells. *Sci. Reports* **2016** *6* (1), 1–10.
- (20) Liao, T.; Yang, Z.; Chen, X.; Chen, J. Thermoradiative-Photovoltaic Cells. *IEEE Trans. Electron Devices* **2019**, *66* (3), 1386–1389.
- (21) Tervo, E. J.; Callahan, W. A.; Toberer, E. S.; Steiner, M. A.; Ferguson, A. J. Solar Thermoradiative-Photovoltaic Energy Conversion. *Cell Reports Phys. Sci.* **2020**, *1* (12), 100258.
- (22) Li, W.; Buddhiraju, S.; Fan, S. Thermodynamic Limits for Simultaneous Energy Harvesting from the Hot Sun and Cold Outer Space. *Light Sci. Appl.* **2020**, *9* (1), 1–11.
- (23) Strandberg, R. Theoretical Efficiency Limits for Thermoradiative Energy Conversion. *J. Appl. Phys.* **2015**, *117* (5), 55105.
- (24) Pusch, A.; Gordon, J. M.; Mellor, A.; Krich, J. J.; Ekins-Daukes, N. J. Fundamental Efficiency Bounds for the Conversion of a Radiative Heat Engine's Own Emission into Work. *Phys. Rev. Appl.* **2019**, *12* (6), 64018.
- (25) Ekins-Daukes, N. J.; Sazzad, M. H.; Kiyumi, L. Al.; Nielsen, M. P.; Reece, P.; Mellor, A.; Green, M. A.; Pusch, A. Generating Power at Night Using a Thermoradiative Diode, How Is This Possible? *47th IEEE Photovolt. Spec. Conf.* **2020**, 2214–2218.
- (26) Santhanam, P.; Fan, S. Thermal-to-Electrical Energy Conversion by Diodes under Negative Illumination. *Phys. Rev. B* **2016**, *93* (16), 161410.
- (27) Wurfel, P. The Chemical Potential of Radiation. *J. Phys. C Solid State Phys.* **1982**, *15* (18), 3967.
- (28) Rau, U. Reciprocity Relation between Photovoltaic Quantum Efficiency and Electroluminescent Emission of Solar Cells. *Phys. Rev. B* **2007**, *76* (8), 085303.
- (29) Jones, R. C. Immersed Radiation Detectors. *Appl. Opt.* **1962**, *1* (5), 607–613.
- (30) Hsu, W. C.; Tong, J. K.; Liao, B.; Huang, Y.; Boriskina, S. V.; Chen, G. Entropic and Near-Field Improvements of Thermoradiative Cells. *Sci. Reports* **2016** *6* (1), 1–10.
- (31) Fiorino, A.; Zhu, L.; Thompson, D.; Mittapally, R.; Reddy, P.; Meyhofer, E. Nanogap Near-Field Thermophotovoltaics. *Nat. Nanotechnol.* **2018** *139* **2018**, *13* (9), 806–811.
- (32) Guha, B.; Otey, C.; Poitras, C. B.; Fan, S.; Lipson, M. Near-Field Radiative Cooling of Nanostructures. *Nano Lett.* **2012**, *12* (9), 4546–4550.

■ NOTE ADDED AFTER ASAP PUBLICATION

This paper was published on May 9, 2022, with the name of a compound written incorrectly in the title. The corrected version was reposted on May 18, 2022.

□ Recommended by ACS

Inverse-Designed Lithium Niobate Nanophotonics

Chengfei Shang, Cheng Wang, et al.

APRIL 06, 2023

ACS PHOTONICS

READ 

Fill Factor Loss in a Recombination Junction for Monolithic Tandem Solar Cells

Johan Lauwaert.

APRIL 06, 2023

ACS APPLIED ENERGY MATERIALS

READ 

Quasi-BIC Modes in All-Dielectric Slotted Nanoantennas for Enhanced Er³⁺ Emission

Boris Kalinic, Giovanni Mattei, et al.

JANUARY 18, 2023

ACS PHOTONICS

READ 

Room-Temperature Continuous-Wave Microcavity Lasers from Solution-Processed Smooth Quasi-2D Perovskite Films with Low Thresholds

Xiang Gao, Lixiang Wang, et al.

MARCH 03, 2023

THE JOURNAL OF PHYSICAL CHEMISTRY LETTERS

READ 

Get More Suggestions >